Polymer 51 (2010) 5255–5266

Contents lists available at ScienceDirect

Polymer

journal homepage: www.elsevier.com/locate/polymer

Characterization of nanoclay orientation in polymer nanocomposite film by small-angle X-ray scattering

Pranav Nawani [a], Christian Burger [a], Lixia Rong [a], Benjamin Chu [a], Benjamin S. Hsiao [a,*], Andy H. Tsou [b], Weiqing Weng [c]

[a] Chemistry Department, Stony Brook University, Stony Brook, NY 11794-3400, USA
[b] ExxonMobil Research and Engineering Company, Annandale, NJ 08801, USA
[c] Butyl Polymers Technology, ExxonMobil Chemical Company, Baytown, TX 77522-5200, USA

ARTICLE INFO

Article history:
Received 13 April 2010
Received in revised form
9 August 2010
Accepted 21 August 2010
Available online 29 September 2010

Keywords:
Nanocomposite
Organoclay
Orientation

ABSTRACT

The orientation distribution of layer-shaped nanoclays (e.g. organoclays and pristine clays) dispersed in a polymer matrix is an important parameter to control the properties of polymer nanocomposites. In this study, we demonstrate that the use of multi-directional 2-D small-angle X-ray scattering (SAXS) can quantitatively describe the orientation distribution of organoclays (e.g. Cloisite C20A) in melt-pressed nanocomposite films, containing ethylene-vinyl acetate (EVA) copolymers as polymer matrices. Different weight fractions of organoclays were used to alter the orientation profile of nanocomposite films, in which the dispersion and morphology of organoclays were also characterized by complementary 2-D and 3-D transmission electron microscopy (TEM). All nanocomposites exhibited mixed intercalation/exfoliation clay morphology, where the intercalated structure possessed partial orientation parallel to the in-plane direction of the film. The higher content of the clay loading showed a higher clay orientation. A simple analytical scheme for SAXS data analysis to determine the orientation parameter (P_2) was demonstrated, the results of which are in agreement with the gas permeation properties of the nanocomposite films.

1. Introduction

Mechanical, gas barrier, flame retardation and other properties of polymers can be significantly altered by incorporating filler particles. If at least one dimension of the particle is in the nanometer range, the composites formed are known as nanocomposites. In the past decade, usage of layer-shaped inorganic fillers, such as pristine clays and organically modified clays (organoclays), for enhancing the properties of polymeric material has been of great interest in both scientific and industrial communities [1–6].

Montmorillonite-type clays are among the most commonly used layer-shaped inorganic clays. They are smectite-type clays, having a 2:1 layered structure i.e., a single octahedral silicate sheet is present between two tetrahedral sheets [7,8] in each layer of the stack. Size and surface area of fillers strongly influence the alteration of the properties [9–11]. Higher surface areas can be achieved by larger aspect ratios; defined as the ratio of the stack lateral dimension to the stack height. The highest possible surface area, of course, is achieved if the clay stacks are completely exfoliated into individual layers upon dispersion in the polymer matrix. To achieve a maximum dispersion of clays, it is imperative that their surfaces are compatible with the polymer matrix. To make montmorillonite compatible with most polymers, a surface modification is performed via exchange of monovalent ions (e.g. Na^+) present in the inter-layer or gallery spaces with organic surfactants, usually primary alkyl ammonium compounds [12]. These clays are often termed as “organoclays” or “organosilicates” [7]. The incorporation of surfactant in between the layers results in an increase in the inter-layer spacing and a decrease in the aspect ratio of the clay stack. However, the increase in *d*-spacing can also facilitate the polymer chains to penetrate into the gallery and exfoliate the stack [1–4].

The lamellar structure of clay stacks in nanocomposites can be characterized by small-angle X-ray scattering (SAXS) [13–16]. However, a quantitative characterization of the stack morphology, especially the degree of clay exfoliation and the orientation of intercalated clay stacks, is rarely performed [17–19]. Thus far, the demonstrated scattering works on nanocomposites mainly focused on the information about the layer periodicity and gallery spacing [20,21]. Disappearance of discrete SAXS peaks is often interpreted in terms of the exfoliation of the clay stack [22], but there could be other

* Corresponding author. Tel.: +1 631 632 7793; fax: +1 631 632 6518.
E-mail address: bhsiao@notes.cc.sunysb.edu (B.S. Hsiao).

0032-3861/$ – see front matter © 2010 Elsevier Ltd. All rights reserved.
doi:10.1016/j.polymer.2010.08.048

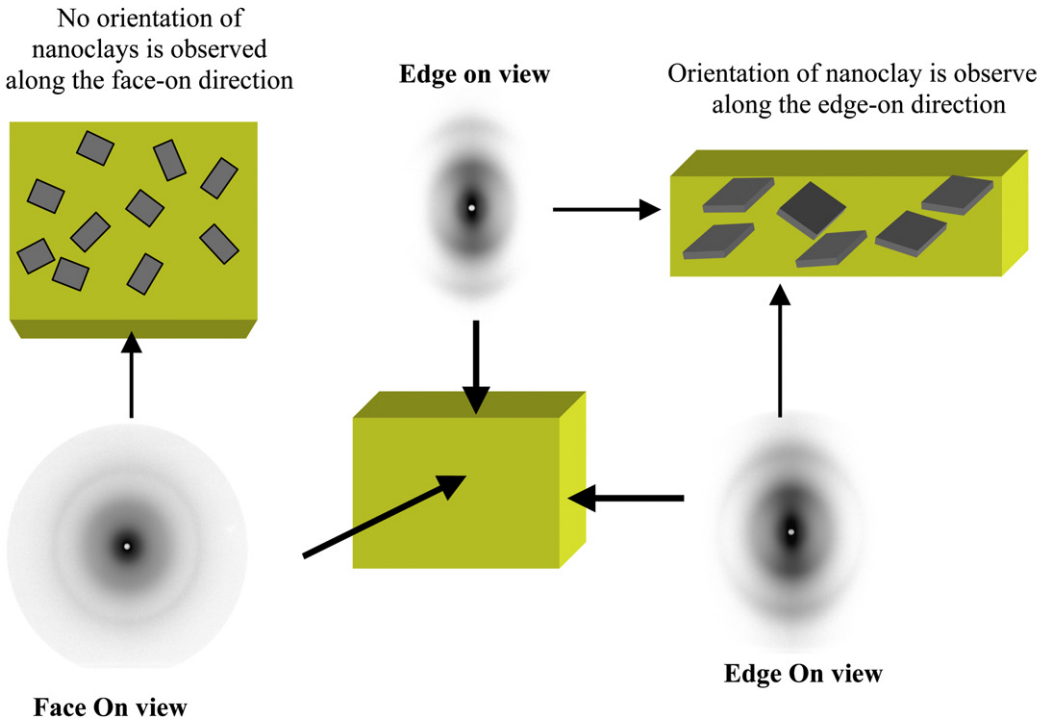

Fig. 1. Sketch of directional 2-D SAXS patterns obtained from typical nanocomposite film with preferred nanoclay orientation.

factors that would cause these peaks to disappear. One of the possible factors is preferred orientation, i.e., a preferred in-plane alignment of the clay platelets in the polymer film plane would drastically decrease the discrete scattering signals along the normal film direction. The relatively high rigidity of clay stacks does indeed result in the preferred alignment of the layered silicates in the polymer film plane by routine film processing procedures (e.g. melt-pressing, calendaring and film blowing); this behavior has been confirmed by several recent scattering studies [17–19]. Preferred orientation of organoclays can be observed in X-ray scattering patterns recorded with 2-D position-sensitive detectors [23]. However, the observed degree of clay orientation is usually not very high in these samples, probably because the very large aspect ratio of the clay platelets can cause them to bend and fold. The effective aspect ratio of clays is thus significantly lower than the ideal aspect ratio.

The effective aspect ratio of the clay particles in polymer nanocomposites can be estimated by a gas permeability experiment [24]. The principle of the experiment is straightforward. The presence of impermeable inorganic filler particles reduces the available free volume to the permeant molecule, whereas the average random walk-like path in which the molecule has to travel within the polymer matrix is increased, thus reducing the gas permeability. The permeation of a molecule in the polymer matrix is dependent on the tortuousity, τ ($=\lambda'/\lambda$, defined as the ratio of the actual distance a molecule must travel to get through the film (λ') to the thickness of the film (λ)) [25]. In polymer nanocomposites with mixed intercalated-exfoliated organoclay morphology, the permeation of gas molecules depends strongly on the extent of dispersion, exfoliation and preferred orientation of the organoclay. A preferred in-plane alignment of the organoclay (stacks or individual sheets) with respect to the film plane increases the tortuousity for the permeating molecule, whereas a preferred perpendicular alignment of the organoclays would decrease the tortuousity (especially when the surfactant layer has lower free volume). If the organoclays are partially exfoliated, their surface area increases, providing more impermeable surfaces, and the tortuousity for permeant molecules will also increase. Thus, in order to increase the tortuousity, the organoclays should exhibit a higher degree of exfoliation and in-plane orientation.

Commercial organoclays based on montmorillonites are effectively agglomerates of smaller, primary stack particles consisting of 10–20 layers in a co-planar orientation. Those primary stack particles are usually referred to as "tactoids," having effective aspect ratios of 10–30 (the effective aspect ratio of an exfoliated organoclay sheet is about 200) [26]. The typical tactoid of mica has an aspect ratio of 30–100, of talc has an aspect ratio of 5–20, and of kaolin has an aspect ratio of 4–12 [27]. Experimentally, it has been demonstrated that the barrier properties of a polymer could be significantly improved with just a few percent of exfoliated high aspect-ratio silicates [28–31]. Without considering the possible changes in the local permeability values due to molecular-level transformation by the presence of silicates, this permeability reduction simply arises from the increase in diffusion path lengths. Nielsen developed a simple model to determine the reduction in permeability in a polymer by accounting for the increase in tortuousity with impermeable and planarly oriented plate-like fillers [32].

$$B/B_0 = (1-f)/(1+af/2) \tag{1}$$

where B is the permeability, B_0 is the permeability of the polymer without fillers, f is the filler volume fraction, and a is the platelet aspect ratio. Cussler et al. [33] and Fredrickson and Bicerano [34] have provided further refinements of this model by removing the positional order, but still having perfect orientation. Recently, Gusev and Lusti [35] conducted a direct three-dimensional finite-element permeability calculation with a model comprised of randomly dispersed, perfectly oriented, and non overlapping platelets. They found all their numerical simulated permeability values could be well represented with a stretched exponential function as

$$B/B_0 = \exp\left[-(af/3.47)^{0.71}\right] \tag{2}$$

The same finite-element simulation approach has been applied to 3-D randomly oriented platelets in the dilute, semi-dilute, and

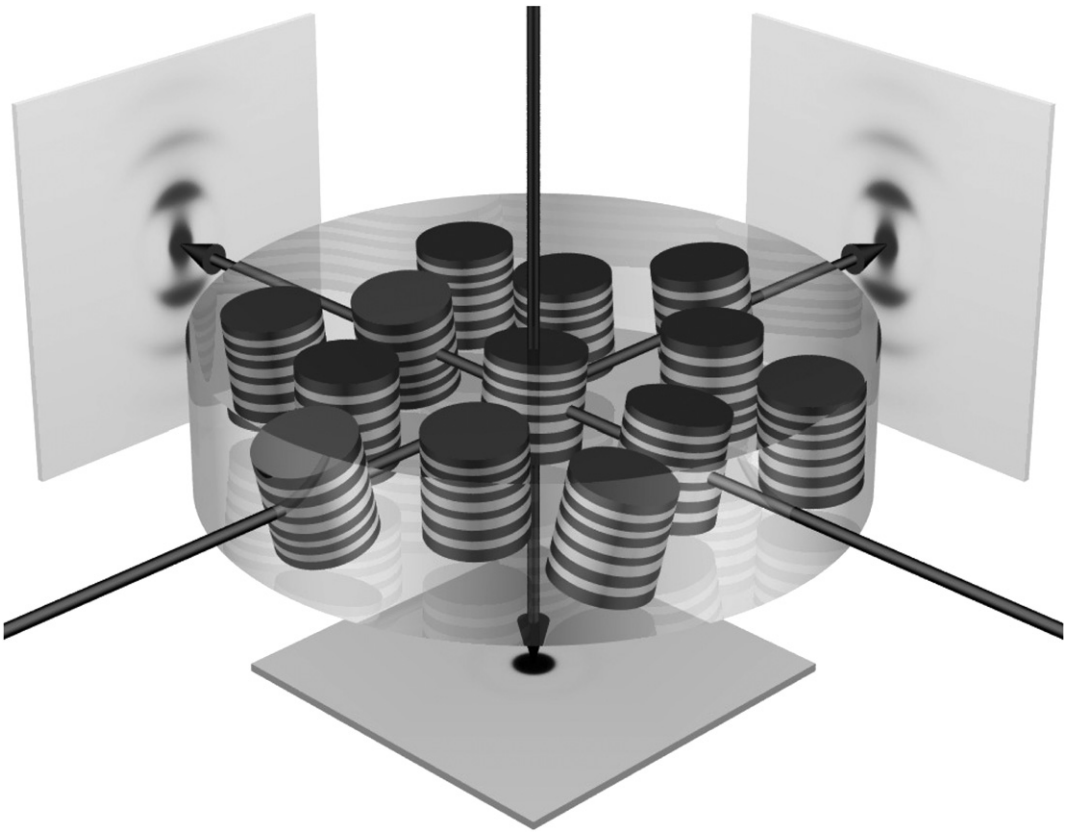

Fig. 2. Directional 2-D SAXS images simulated from disk-like nanoclays with cylindrical symmetry and preferred orientation.

concentrated regimes [36]. The relative permeability of composites consisting of misaligned disks was determined as a function of the aspect ratio of the inclusions. Although the model of misaligned platelets has been applied successfully in representing the actual experimental data [37,38] and in extracting a macroscopic volume-average aspect ratio of the inclusions, the lack of a simple mathematical form renders its application difficult.

In this study, we demonstrate an analytical scheme that can quantitatively determine Hermans' orientation parameter (P_2) of intercalated clay stacks (or tactoids) from a 2-D SAXS image. The results were checked with 3-D simulation of SAXS profiles using a tactoid model as well as 3-D transmission electron microscopy (TEM) of a real sample for consistency. We note that this method does not address the issue of clay dispersion but determines the preferred orientation of the intercalated stacks only. Furthermore, we assumed that the clay dispersion (i.e., the ratio between exfoliated and total clay fraction) in the chosen nanocomposite samples, containing the same chemical composition of organoclays but different loading content, was about the same under the chosen melt-mixing conditions (this was checked with 2-D TEM measurements). Under this assumption, the measured gas permeability and the calculated effective aspect ratio using Eq. (2) were compared with the estimated Hermans' orientation parameter of the intercalated clay stacks to check the consistency of the SAXS analysis.

2. Experimental

2.1. Materials and sample preparation

Ethylene-vinyl acetate (EVA) copolymers were chosen as the polymer matrices, which were received from DuPont Company. Two types of EVA samples were used: Elvax350, having 25 wt% (~8 mol%) of vinyl acetate and a melt index of 19 (ASTM D1238); Elvax770 having 9.5 wt% (~3 mol%) of vinyl acetate and a melt index of 0.8. Both EVA samples were structurally similar to low-density polyethylene (LDPE) with many chain branches, and their density values were about 0.94 g/cm^3. The organoclay used was Cloisite 20A (C20A) from Southern Clay Company. This organoclay was based on montmorillonite from Wyoming Cloisite containing the surfactant dimethyl di-hydrogenated tallow ammonium chloride. The surfactant content in C20A was ~35 wt% according to the manufacturer and our thermogravimetric analysis [39]. The interlayer gallery spacing in C20A at room temperature, determined by SAXS, was 2.4–2.6 nm. The C20A sample was dried in vacuum for 24 h at room temperature prior to its usage.

Nanocomposites were prepared by melt blending EVA350 or EVA770 copolymers with different amounts of organoclay (C20A) using a micro-processor (DACA, US). The combined weight of organoclay and polymer was 3.0 g per load. Two organoclay concentrations were prepared: 5 wt% and 10 wt%. Melt mixing was performed at 170 °C at 200 RPM under the flow of nitrogen. To achieve sufficient clay dispersion, the mixing time was 10 min. After mixing, the polymer nanocomposite was extruded and subsequently pressed by a Carver pressing apparatus at 170 °C and 4000-psi pressure. Samples were left to anneal for 30 min at 170 °C and then cooled down to room temperature. The typical size of the polymer nanocomposite film made for the X-ray measurements was 4 mm × 4 mm with 1 mm thickness.

2.2. 2-D and 3-D transmission electron microscopy

All nanocomposite samples were cryo-microtomed at −150 °C using a diamond knife to obtain sections of 100 nm thickness for transmission electron microscopy (TEM) measurements. No

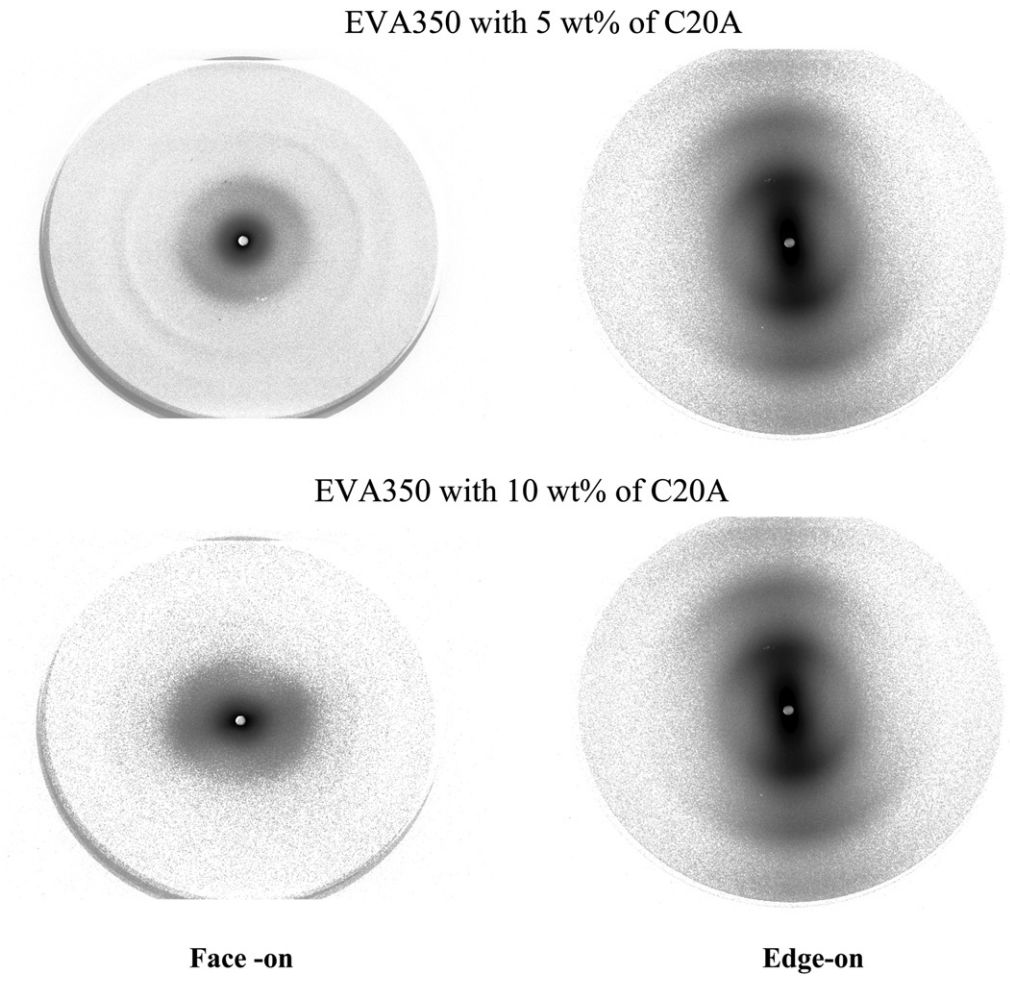

Fig. 3. Directional 2-D SAXS patterns obtained from two EVA350/C20A nanocomposites with different organoclay loading.

staining was applied. 2-D TEM images were acquired on a JEOL 2000FX TEM instrument at 160 kV accelerating voltage. Multiple images from various locations at different magnifications were collected to provide an overall assessment of the dispersion uniformity and clay morphology. For 3-D TEM, an FEI Tecnai TEM instrument (G2 F20 Super Twin TMP) was used. All samples were run on the scanning transmission electron microscopy high-angle annular dark field (STEM-HAADF) mode to minimize the sample damage while maximizing the contrast. The image acquired in such a way is also known as STEM-HAADF tomography. During the measurements, the sample was tilted from a 0° angle to −60°, which took about 90 min, and the samples were tilted back from 0 to 60°, which took another 90 min. The total exposure time was 3 h. The images were reconstructed using the Voltex 3-D volume rendering software.

2.3. Synchrotron small-angle X-ray scattering

Small-angle X-ray scattering (SAXS) measurements were performed at the X27C beamline at the National Synchrotron Light Source (NSLS), Brookhaven National Laboratory (BNL). The X-ray wavelength was 1.371 Å. Silver behenate was used to calibrate the

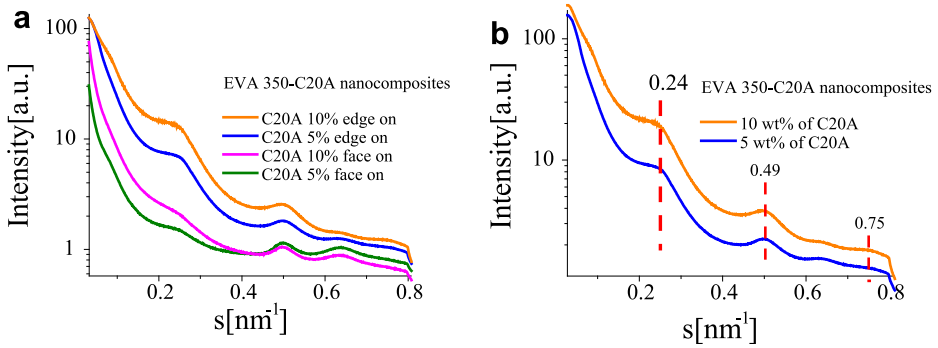

Fig. 4. (a) Integrated SAXS profiles of EVA350/C20A nanocomposites with various weight fractions of C20A taken at different sample orientation. (b) Comparison of edge-on SAXS profiles from EVA350/C20A nanocomposites as a function of C20A loading.

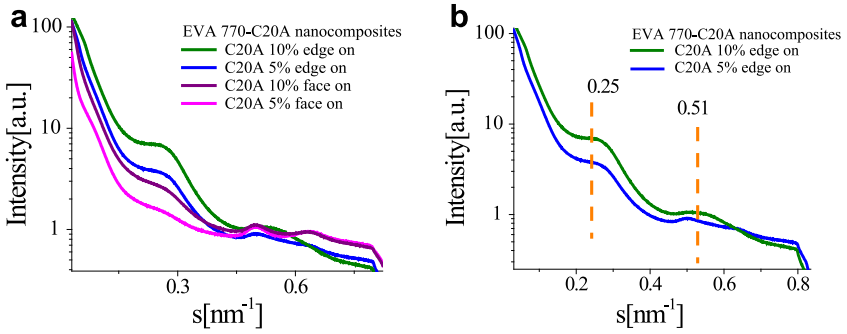

Fig. 5. (a) Integrated SAXS profiles of EVA770/C20A nanocomposites with various weight fraction of C20A taken at different sample orientation. (b) Comparison of edge-on SAXS profiles from EVA770/C20A nanocomposites as a function of C20A loading.

scattering angle in SAXS. X-ray measurements for all nanocomposite samples were taken under the same conditions, i.e., three SAXS images were taken from each sample by changing the orientation of the film with respect to the X-ray beam. The direction of the beam hitting the sample, normal to the plane of film is called "face-on" direction, and if parallel to the plane of film it is called "edge-on" direction. These directions are shown in Fig. 1. 2-D SAXS patterns were acquired using imaging plates manufactured by Fuji Company. 1D SAXS profiles were obtained by integrating 2-D images using the Polar software (Stonybrook Technology and Applied Research (STAR), Inc., Stony Brook, NY) [23]. The sample-to-detector distance for SAXS was 820 mm. All scattering/diffraction signals were corrected for beam fluctuations, sample absorption and background scattering. We note that the edge-on images taken at different orientations were near identical, indicating that the melt-pressed film had a (fiber) cylindrical symmetry.

2.4. Permeability test

EVA-C20A nanocomposites were compression-molded into films at 150 °C. Five-centimeter diameter disks were punched out from these molded films and conditioned in a vacuum oven at 40 or 60 °C overnight prior to the permeability measurements. Oxygen permeation values at 40 °C for polymer nanocomposite films were acquired using a Mocon OX-TRAN 2/61 permeability tester.

3. Results and discussion

3.1. Hermans' orientation function of nanoclays determined by SAXS

We assume the individual nanoclay stack possesses cylindrical symmetry about its stack axis, and the axes of all the nanoclay stacks are preferentially oriented with respect to the film normal. In other words, the film possesses fiber symmetry as illustrated in Fig. 2. In this case, the preferred orientation of the nanoclay stacks can be described by an orientation distribution function $g(\beta)$ depending on a single angle β that is the angle between the individual stack axis (or the layer normal) and the film normal. For the edge-on scattering geometry, we will refer to the vertical (i.e., film normal) direction as the "meridional" direction and the horizontal direction as the "equatorial" direction. For a system with moderate orientation of nanoclay stacks, the meridional scattering in the edge-on SAXS is arc-like (Fig. 1), which can be factored into a radial and an angular component. The latter can be used to determine the orientation distribution of nanoclays dispersed in the polymer matrix.

The relationships between the intensity distribution of the structural unit (i.e., individual nanoclay stack), $I(s,\varphi')$, the intensity distribution of the nanocomposite film sample, $J(s,\varphi)$, and the orientation distribution, $g(\beta)$, can be given by the following integral transformation given by Ruland [40,41]:

$$J(s,\phi) = \int_0^{\pi/2} I(s,\phi')F(\phi,\phi')\sin\phi' d\phi' \tag{3}$$

where $F(\varphi,\varphi')$ depends on $g(\beta)$ given by another integral transformation.

$$F(\phi,\phi') = \frac{1}{\pi}\int_0^{\pi} g(\beta)d\eta \tag{4}$$

and the dependency between β and η is given by following equation

$$\cos(\beta) = \cos\phi\cos\phi' + \sin\phi\sin\phi'\cos\eta \tag{5}$$

here φ' is the polar angle in the coordinate system of the individual stack and φ is the polar angle of the ensemble and η is the angle between φ' and φ.

Under certain conditions, the above relationships can be simplified. If an angular profile can be taken at the maximum intensity in the radial direction of the meridional arc from 2-D SAXS, this 1D angular profile (after normalization) is equivalent to the orientation distribution. Note that the same is not true for equatorial or off-axis reflections. The angular profile can be fitted to an orientation distribution function for which we chose a modified Onsager distribution [42].

$$g(\beta) = p_0 + (1-p_0)\times\left(\frac{p}{\sinh p}\right)\times(\cosh(p\cos\beta)) \tag{6}$$

Table 1
Relationship between clay orientation and gas permeability for EVA350/C20A nanocomposite containing various clay loadings.

EVA350/C20A nanocomposite	Permeability	Orientation factor [*P*2]
0 wt% of C20A	53.42	0.00
5 wt% of C20A	42.59	0.14
10 wt% of C20A	36.05	0.31
10 wt% of C20A (from calculated image)		0.33

Table 2
Clay orientation for EVA770/C20A nanocomposite containing various clay loadings.

EVA 770/C20A nanocomposite	Orientation factor [*P*2]
0 wt% of C20A	0.00
5 wt% of C20A	0.12
10 wt% of C20A	0.30

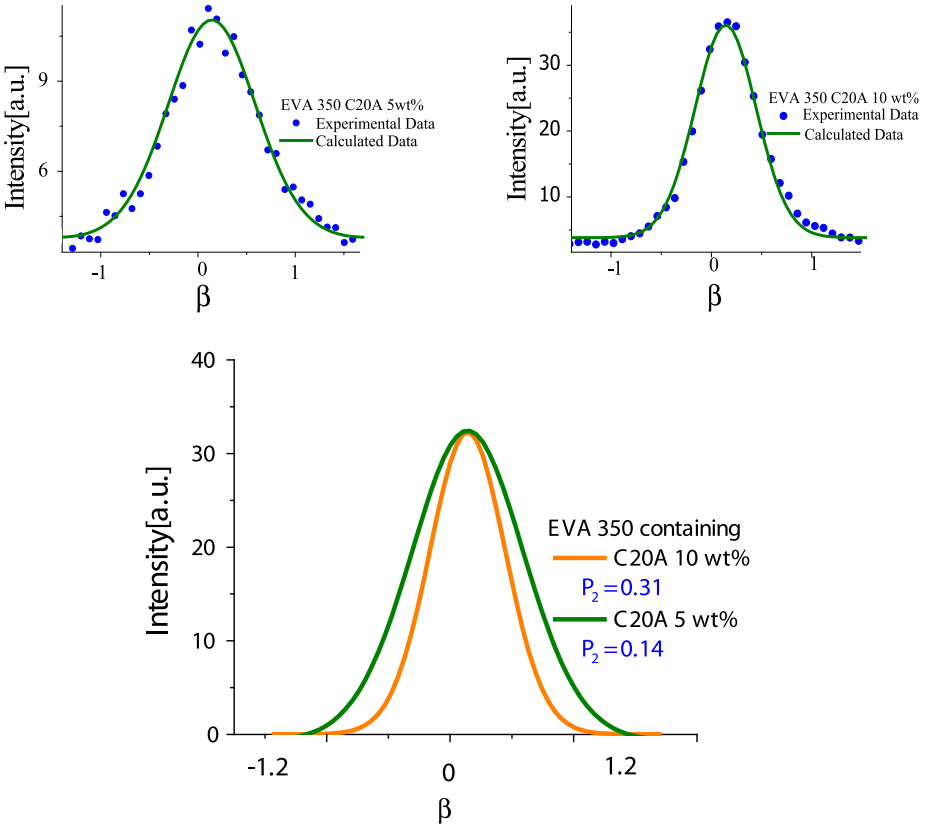

Fig. 6. Experimental and calculated orientation distribution $g(\beta)$, and comparison of two EVA350/C20A nanocomposites with different loading of C20A (5 wt% and 10 wt%).

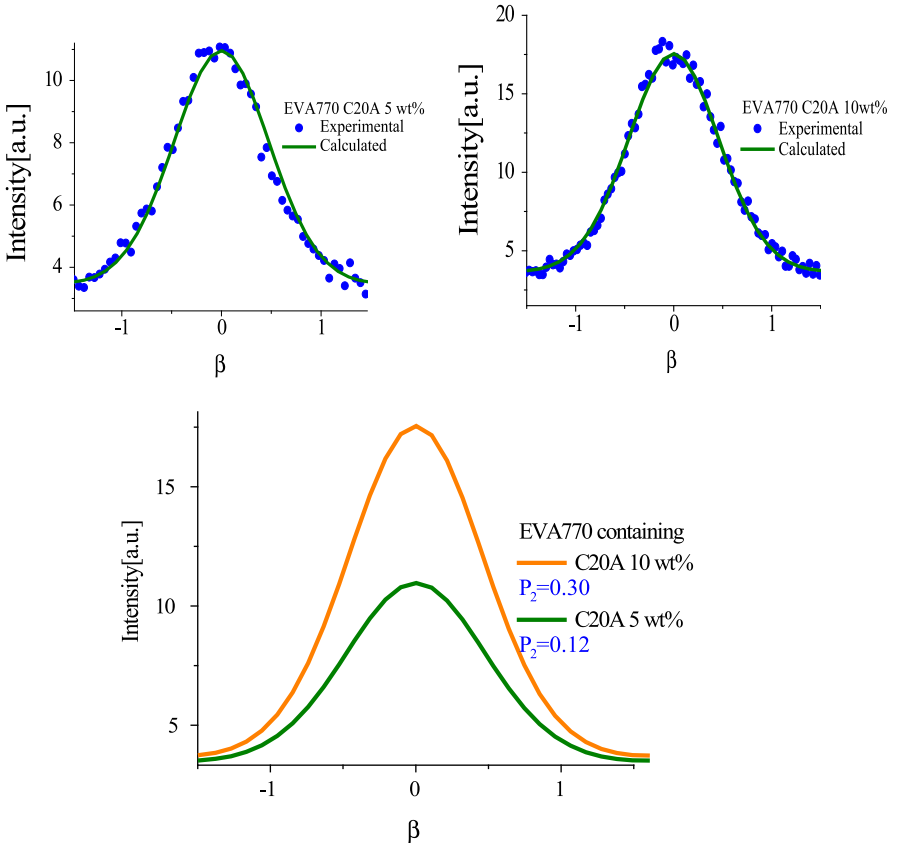

Fig. 7. Experimental and calculated orientation distribution $g(\beta)$, and comparison of two EVA770/C20A nanocomposites with different loading of C20A (5 wt% and 10 wt%).

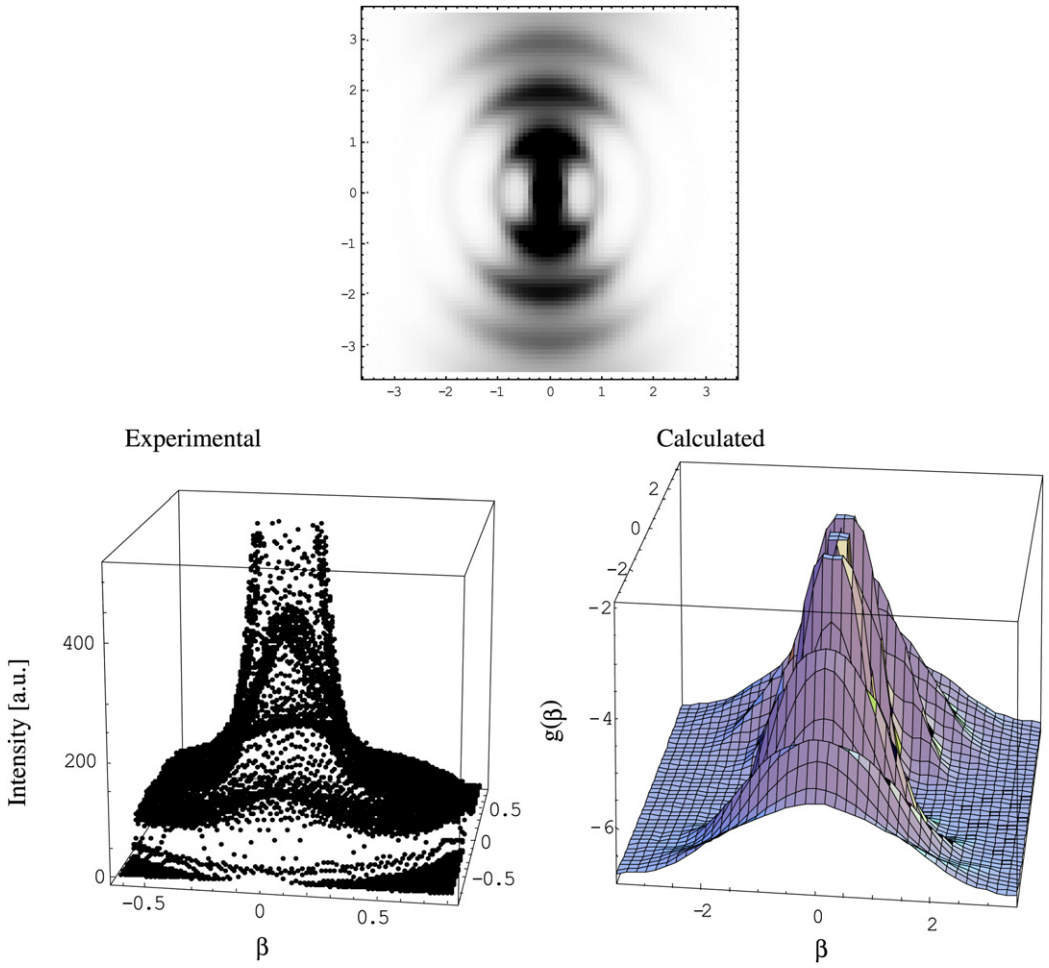

Fig. 8. Comparison of experimental and calculated 2-D SAXS images and corresponding orientation distribution $g(\beta)$ profiles of nanoclay from EVA350-C20A (10 wt%) nanocomposite.

where p is related to the width of the orientational distribution of the nanoclay stacks in the nanocomposite system (the higher the p value, the higher the degree of nanoclay orientation). The p value can range between zero and infinity (p is 0 for isotropic system). The parameter p_0 represents an isotropic contribution, and its value lies between 0 and 1. For an unoriented system with "$p = 0$", $g(\beta)$ does not depend on p_0.

The width of the orientation distribution (thus the extent of the preferred orientation of nanoclay stacks) can be quantified using the Hermans' orientation parameter [43]:

$$\overline{P}_2 = 0.5 \times \left[3 \times \frac{\int_0^{\pi/2} g(\beta)\cos^2(\beta)\sin(\beta)d\beta}{\int_0^{\pi/2} g(\beta)\sin(\beta)d\beta} - 1 \right] = (1-p_0)\left(1 - 3p^{-1}\left[\coth(p) - p^{-1}\right]\right) \quad (7)$$

Thus, the angular profile taken at the maximum radial scattering intensity can be fitted by the Onsager expression (Eq. (6)) to determine Hermans' orientation parameter (Eq. (7)) of the nanoclay orientation in polymer matrix. In the following sections, we will demonstrate the use of this simple approach for the analysis of SAXS data, and to crosscheck its validity with the 3-D SAXS simulation with a simple real space model, as well as with the 2-D/3-D TEM measurements of the tested samples.

3.2. Nanoclay orientation in melt-pressed EVA-C20A nanocomposite films

SAXS measurements of all chosen EVA/C20A nanocomposite films exhibited some common scattering features (as shown in Fig. 1), which seem to be universal for most melt-pressed and solution-cast nanocomposite films containing intercalated nanoclays (i.e., organoclays or pristine clays). These features are as follows. (1) The face-on SAXS image shows little or no nanoclay orientation. (2) All edge-on SAXS images show distinct nanoclay orientation with a near fiber symmetry, i.e., the scattering characteristics (peak positions, intensity ratios, angular spreads) appear to be independent of the edge-on direction. (3) The intercalated clay structure being very distinct along the edge-on direction, but quite vague along the face-on direction. If the edge-on pattern indicates that the degree of preferred orientation of nanoclay is high, the discrete scattering maxima along the face-on direction can completely disappear, leaving the merely appearance of diffuse scattering and the mistaken impression of "exfoliation" (We note that only isotropic SAXS images exhibiting featureless diffuse scattering profiles may be considered the evidence of "exfoliation").

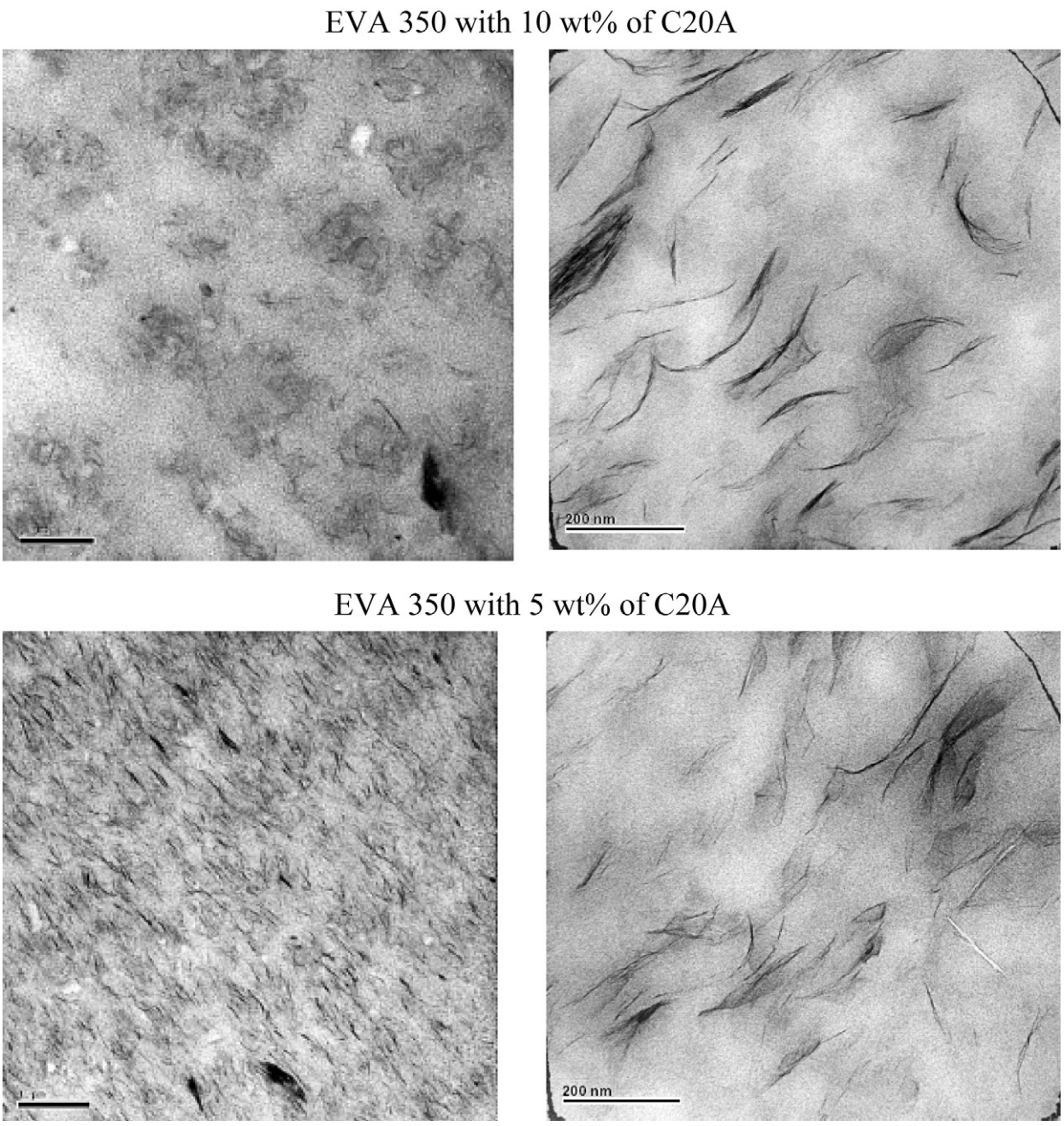

Fig. 9. 2-D TEM images of various weight fraction of C20A dispersed in EVA350 at different magnifications (the left scale bar is 1 μm, the right scale bar is 200 nm).

(4) Although the edge-on SAXS patterns from most melt-pressed films (including some highly processed film samples prepared by blow-molding and slightly melt-pressed film samples at relatively low pressures) all show preferred nanoclay orientation, the observed degrees of clay orientation are never very high when compared with the crystal orientation in processed polymer fibers and films. This may be because the average aspect ratio of the resulting nanoclay particles is relatively low due to bending and folding, which are unavoidable consequences during most processing conditions. However, the change of the filler loading content appears to be an effective way to affect the nanoclay orientation at a moderate level.

Before we discuss results from directional SAXS measurements of nanocomposite films, let us first describe the structures obtained from SAXS studies of organoclays and melt-mixed nanocomposite samples in the absence of mechanical pressing. In the study of as-received C20A organoclay, peak positions in the SAXS profile were non-equidistant, which has been explained by the bimodal thickness distribution of two surfactant layers, where the thicker layers were overloaded by excessive surfactant above the average cation exchange capacity (CEC) [44]. In contrast, the SAXS profiles of all nanocomposite samples, without melt-pressing, showed equidistant scattering peaks, indicating that the excess surfactant in the galleries probably escaped into the polymer matrix. As peak positions decreased in the nanocomposites (i.e., the periodic layer spacing increased), we can further conclude that some polymer chains were diffused into the gallery, resulting in an intercalated layered structure. In addition, a broadening of the scattering peaks was observed, probably due to increased stack disorder or/and partial exfoliation that reduced the stack heights.

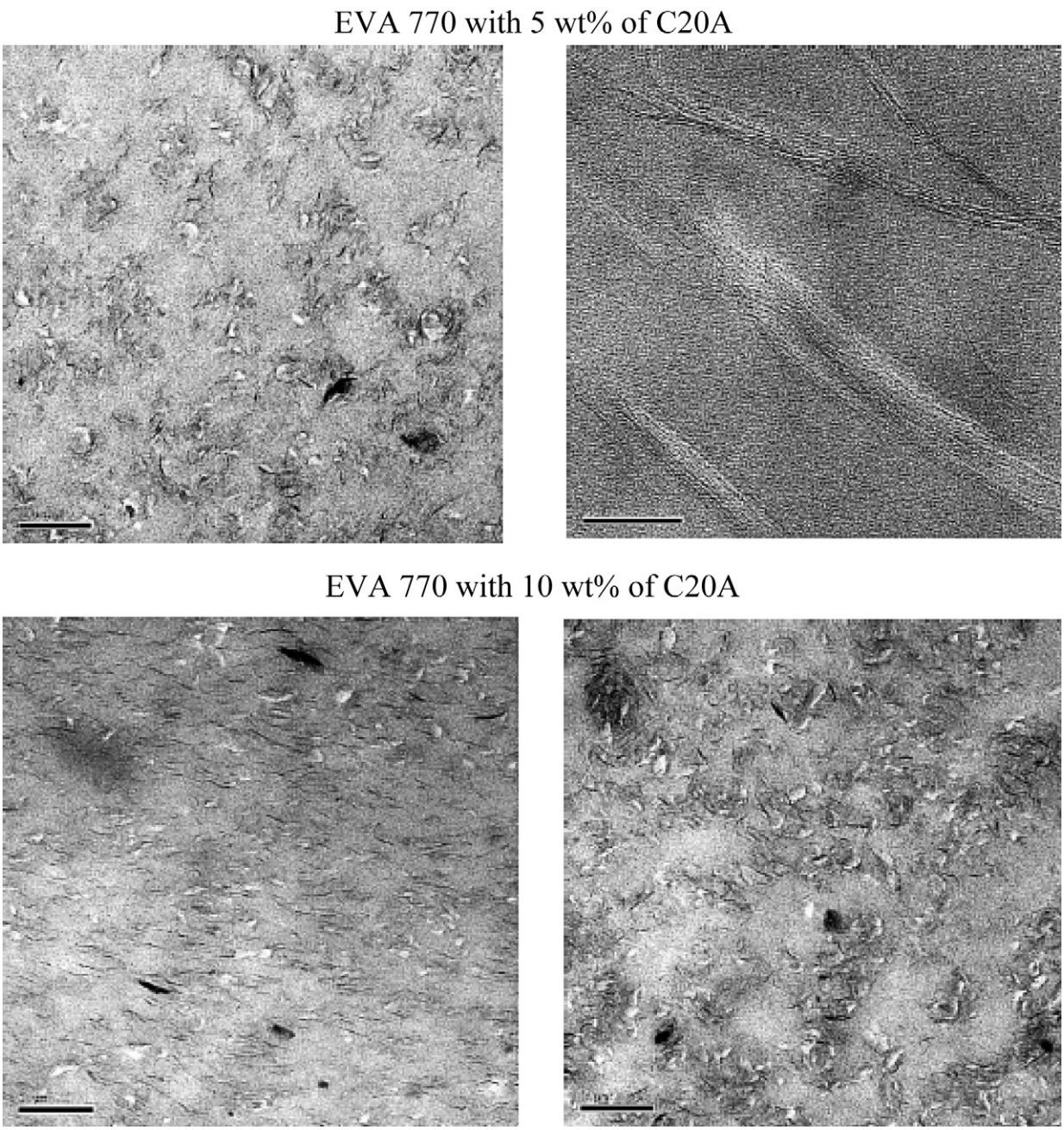

Fig. 10. 2-D TEM images of various weight fractions of C20A dispersed in EVA770 at different magnifications (the left scale bar is 1 μm, the right scale bar is 200 nm).

Fig. 3 illustrates typical directional 2-D SAXS patterns for two EVA350/C20A nanocomposite films of different C20A loadings (5 and 10 wt%). In the edge-on view, multiple arc-shaped scattering peaks in the meridional direction were observed. This scattering feature indicated the presence of clay stacks with preferred orientation as discussed earlier. The absence of any equatorial peaks in the SAXS images in Fig. 5 indicate that there are no clay particles oriented in the direction perpendicular to the plane of polymer film. The observed nanoclay orientation is a result of the melt compression process, while such a scattering feature is hardly observed in extruded samples. Hence, in extruded samples, nanoclays are by and large randomly oriented. The observed 2-D SAXS data was also used to estimate the degree of preferred orientation of the nanoclays using the Hermans' orientation factor. The calculated values of nanoclay orientation based on the Hermans' orientation factor are tabulated in Tables 1 and 2.

In this study, the 2-D SAXS images, collected for two different samples with respect to different X-ray beam direction, are shown in Fig. 1. The results indicated that nanoclay stacks were oriented in the direction parallel to the plane of polymer film. This conclusion was confirmed by integrated SAXS profiles of two types of polymer nanocomposites with different weight fractions of C20A taken at different directions (edge-on and face-on), where the results are illustrated in Figs. 4 and 5. In these figures, the edge-on profiles show distinct scattering maxima positioned at about equal-distance, where the face-on profiles show no sign of scattering maxima in 2-D images (only upon integration, a slight scattering shoulder is observed). The nanocomposite sample with higher nanoclay content shows a more defined feature of scattering maxima and higher scattered intensity. This observation can be explained as follows. Each nanoclay particle has an effective excluded volume. During melt compression, such an excluded

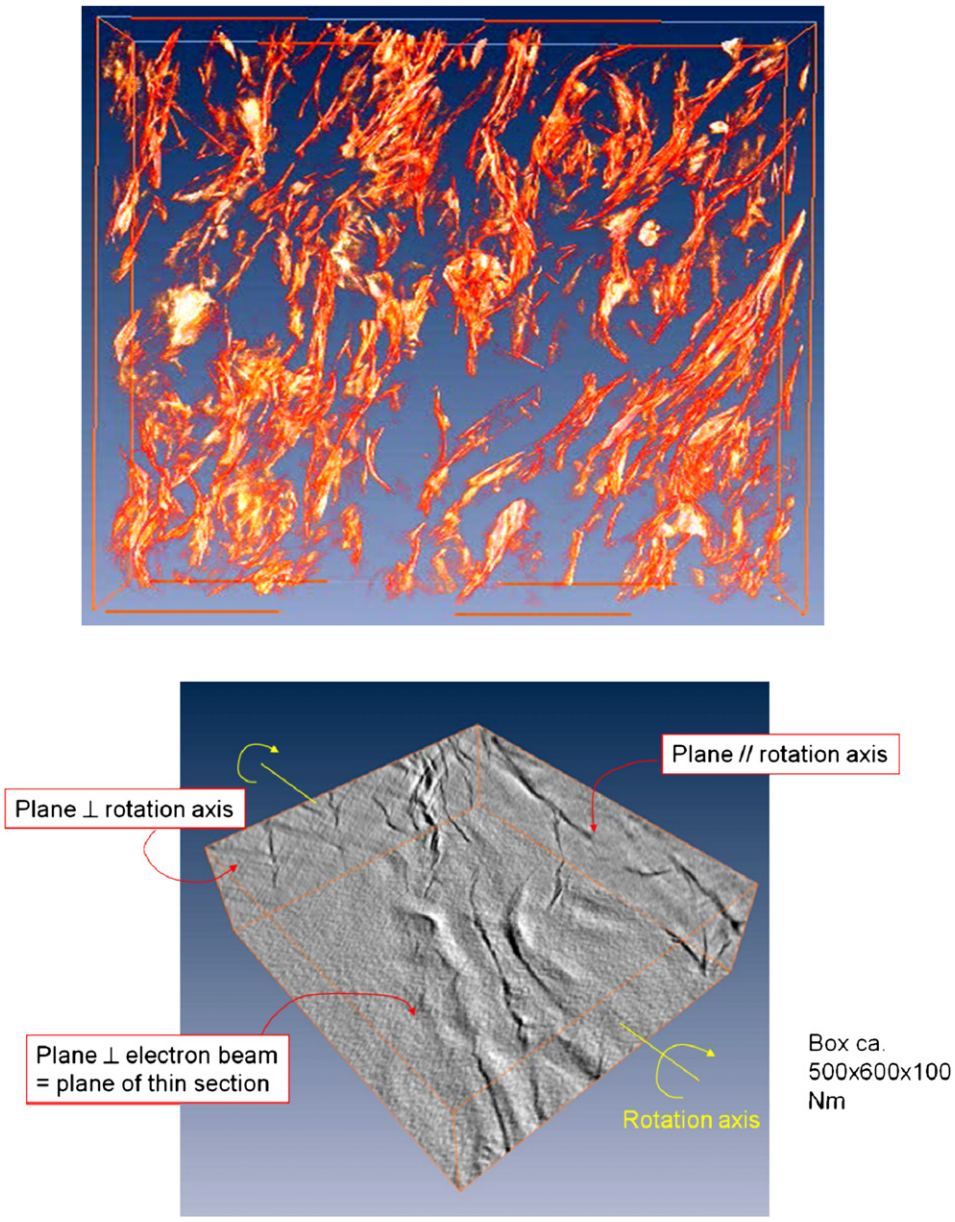

Fig. 11. 3-D TEM image of nanocomposite sample with 10 wt% of C20A dispersed in EVA350.

volume is reduced and the rotation of nanoclay particles becomes restricted. As a result, nanoclay particles tend to align themselves in a direction parallel to the film plane upon compression. The higher the nanoclay content, the less the ability for the nanoclay to rotate, resulting in higher nanoclay orientation. In contrast, in the extrusion process, the rotational restriction of the nanoclay is usually not that severe, such that the resulting nanoclay orientation in the extruded sample can be completely random.

The angular intensity profile, taken at the position of the scattering maximum in 2-D wide-angle X-ray diffraction (WAXD) pattern, has been routinely used to estimate the Hermans' orientation function. However, such an analysis is not applicable to deal with 2-D SAXS data. One research group has used the approach of half width at half maxima to analyze the angular intensity profile and calculate the orientation parameter. Unfortunately, no theoretical base can be established for their analysis. In this study, the Herman's orientation factor ($\overline{P}_2$), given by Equation (8), was used to estimate the degree of preferred orientation of nanoclay in the polymer matrix from the edge-on patterns, in which a sound theoretical background is based. It is well known that, in a completely oriented system, the value of $\overline{P}_2$is 1, while for a completely random system this value is 0. The analysis of orientation distribution profiles for EVA350/C20A and EVA770/C20A nanocomposites are shown in Figs. 6 and 7, respectively, where the measured and calculated intensity profiles are compared. It was found that with the increase in the weight fraction of nanoclay, the

Table 3
Equivalent projected aspect ratios of Cloisite C20A in varying EVA polymer matrix.

EVA	wt% of C20A	Permeability ratio	Equivalent aspect ratio	Average aspect ratio
EVA350	55	0.79	13	22
EVA350	10	0.49	32	22
EVA770	5	0.81	11	15
EVA770	10	0.60	19	15

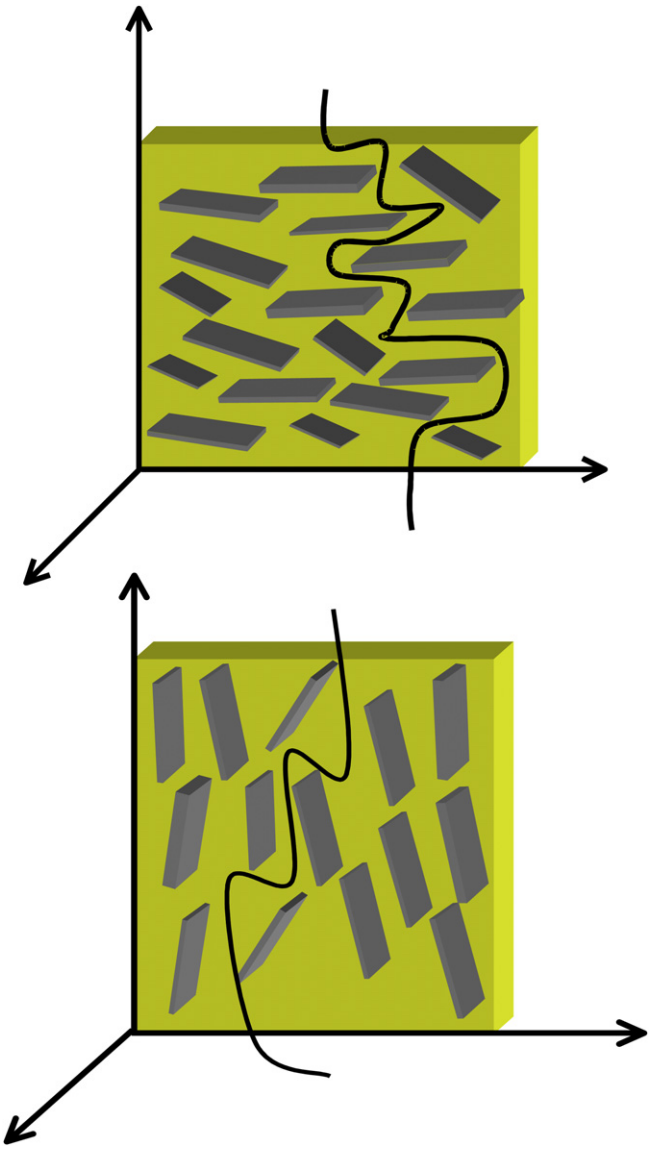

Fig. 12. Schematic diagram of gas tortuousity when organoclays have different degree of orientation.

higher orientation factor ($\overline{P}_2$) of nanoclay was obtained. This observation further complies with our hypothesis that the free volume available for the nanoclay particles to rotate decreases with the increase of nanoclay loading, leading to an increase in nanoclay orientation under the same compression conditions. To check the consistency of this analysis, the entire 2-D SAXS image was analyzed, which yielded a consistent orientation factor ($\overline{P}_2$) as reported. The comparison of experimental and calculated 2-D SAXS images and their corresponding 3-D orientation distribution $g(\beta)$ profiles of nanoclay from the EVA350-C20A (10 wt%) nanocomposite is shown in Fig. 8. It can be seen that the measured and calculated 2-D SAXS patterns are in good agreement.

3.3. Transmission electron microscopy (TEM)

The SAXS profile showing multiple scattering maxima at relatively large spacing indicates that polymer chains have intercalated into nanoclay galleries. Disappearance of the scattering maxima could mislead to the conclusion that the clay stack is completely exfoliated. As a result, microscopic evidence of the morphology of the nanocomposite is welcome to help drawing a conclusion related to the nature of the clay arrangement. TEM images of various weight fraction of clay dispersed in two different polymer matrices (EVA350 and EVA770) are shown in Figs. 9 and 10. These images reveal that there is no large aggregation of nanoclay stacks in either of the polymer matrices, hence indicating the homogeneous dispersion of nanoclays in the polymer matrix. This also holds true for weight fraction as high as 30-wt% of nanoclays dispersed in EVA polymer matrix. At lower magnification of the TEM image, the nanoclays appear to be well dispersed in the polymer matrix. On increasing the magnification of these images, we see the presence of individual silicate layers, all across the polymer matrix and some stacks of clay are visible suggesting partial exfoliated nanostructure. During the process of melt mixing, the polymer chains penetrate in between the layers of the nanoclays and break them into tactoids; and in doing so, individual silicate layers can be torn apart from the stack due to mechanical force. These individual silicate layers may be loosely held depending on the interaction of surfactants with the silicate layer. As surfactants are dispersed in nanoclays (they replace the inter-layer ion of silicates), there is the possibility that not each of the silicate layers is being held by similar electrostatic forces. Hence, layers with weaker electrostatic interaction can fall apart during intercalation of polymer chains. It is quite clear from the 2-D TEM images that the possibility of partial exfoliation is higher when the weight fraction of polymer is higher. This is because more chains are available for penetration through the inter-layer spacing of the nanoclays, resulting in a higher probability of exfoliation. This argument can also explain the observation for the change in scattering features of organoclays when dispersed in polymer nanocomposites, even though there is not much difference in dispersion at higher weight fractions of nanoclays, and there appears to be no aggregation of mineral. To confirm the dispersion and partial exfoliation of nanoclays in the polymer matrix, a 3-D TEM image of one of the nanocomposites samples (10 wt% of C20A dispersed in EVA 350) is shown in Fig. 11. This image shows that there are no large overlapping effects, and the spatial distribution provides an estimate of the dispersion state, which is consistent with our earlier assessment based on SAXS and 2-D TEM results.

3.4. Permeability and projected equivalent aspect ratio

The projected equivalent aspect ratios as calculated from Equation (2) for organoclay with various weight fractions of C20A dispersed in EVA350 and EVA770 are tabulated in Table 3. A progressive increase in the aspect ratio with increased loading reflects the observed increase in planar orientation of C20A in EVA from TEM micrographs. The orientation effect with increased loading of nanoclay seems to be stronger in EVA350 than that in EVA770. This observation again seems to be in agreement with findings from the TEM micrographs. Taking the average aspect ratio and averaging over the values obtained for different C20A concentrations, EVA350 appears to disperse C20A better than EVA770. As EVA350 contains 8 mol% of vinyl acetate and EVA770 contains 3 wt%, EVA350 is more polar, hence resulting in better dispersion of C20A organoclay.

It is well known that both morphology and particle orientation play a very important role in affecting the permeability of the system. The results indicate that there was a reduction in permeability by 20.3% at 5-wt% of clay loading and 32.5% at 10-wt% of clay loading. The decrease in permeability with increasing clay content can be explained by enhanced preferred orientation, which increases with clay loading. The increase in in-plane clay orientation results in greater tortuousity, whereby creating a more tortuous

path for permeating molecule to travel through the system. A sketch in Fig. 12 shows the random walk path traveled by the permeating molecule in a system with orientation perpendicular and parallel to the polymer film, respectively. It is clear that the increase of nanoclay orientation along the in-plane direction of polymer film results in an increase of a tortuous path for permeating molecule. Such observations are consistent with both SAXS and TEM results.

4. Conclusions

A directional SAXS analysis technique along with complementary TEM measurements was used to characterize the orientation of a Cloisite 20A organoclay dispersed in the EVA polymer matrix. The effect of weight % on the orientation (i.e., Hermans' orientation parameter) of dispersed clay was discussed and a qualitative relationship between orientation and permeability was established. From the TEM investigation, the morphology of polymer nanocomposites was found to be a mixture of exfoliated and intercalated structures. The mixed morphology, consisting of tactoids with a stack height distribution and individual clay platelets, is dependent of the processing conditions. The resulting clay structures retain some parallel registry with respect to the film direction, where the directional SAXS technique can be used to quantify the orientation distribution of dispersed organoclays in polymer matrix. In melt-pressed nanocomposite films, the edge-on SAXS pattern exhibits fiber symmetry, allowing the orientation distribution of organoclays in the in-plane direction to be estimated using an analytical approach. It is found that the increase in organoclay fraction in the polymer matrix enhances the clay orientation. This can be explained by the decrease of available free volume leading to the restriction of rotation for organoclay particles. The presence of exfoliated layers and oriented stacks can effectively create a tortuous pathway for a permeating molecule, resulting in a longer distance traveled and more time taken. Although we did not obtain ideally oriented and exfoliated layers parallel to plane of film, the orientation created by clay stacks and the mixed intercalated/exfoliated clay structures were sufficient to create a deviating path for the permeating molecule. Hence, it can be said that exfoliation and orientation of organoclays together are the two most effective factors for the improvement of gas permeation properties in polymer nanocomposites."

Acknowledgement

The authors wish to thank the National Science Foundation (DMR-0906512) and a grant from the ExxonMobil Chemical Company for the financial support. The assistance of Drs. Lixia Rong and Jie Zhu for synchrotron SAXS experimental setup is also greatly appreciated.

References

[1] Giannelis EP. Adv Mater 1996;8(1):29.
[2] Blumstein A. J Polym Sci Part A 1964;3(7):2665–72.
[3] Kojima Y, Usuki A, Kawasumi M, Okada A, Karauchi T, Kamigaito O. J Polym Sci Part A 1993;49:1259–64.
[4] Giannelis EP. JOM 1992;44:28.
[5] Gleiter H. Adv Mater 1992;4(7–8):474–81.
[6] Novak BM. Adv Mater 1993;5(6):422–33.
[7] Scott MA, Carrado KA, Dutta PK. Handbook of layered materials; 2004.
[8] Ray SS, Okamoto M. Prog Polym Sci 2003;28:1539–641.
[9] Thostenson E, Li C, Chou T. J Composites Sci Technol 2005;65:491–516.
[10] Schmidt D, Shah D, Giannelis EP. Solid State Mater Sci 2002;6(3):205–12.
[11] Luo JJ, Daniel IM. Compos Sci Technol 2003;63(11):1607–16.
[12] Schmidt D, Shah D, Giannelis EP. Curr Opin Solid State Mat Sci 2002;6(3):205–12.
[13] Walker GF. Clay Miner 1967;7:129–43.
[14] Johns WD, Gupta PKS. Am Mineral 1967;52:1706–24.
[15] Xie W, Gao ZM, Pan WP, Hunter D, Singh A, Vaia R. Chem Mater 2001;13:2979–90.
[16] Vaia RA, Teukolsky RK, Giannelis EP. Chem Mater 1994;6:1017–22.
[17] Bafna A, Beaucage G, Mirabella F, Mehta S. Polymer 2003;44(40):1103–15.
[18] Hongladarom K, Ugaz VM, Cinader DK, Burghardt WR, Quintana JP, Hsiao BS, et al. Macromolecules 1996;29(16):5346–55.
[19] Dadmun MD, Han CC. Macromolecules 1994;27:7522–32.
[20] Reynolds RC. In: Brindley GW, Brown G, editors. Interstratified clay minerals. London: Mineralgical Society; 1980. p. 249–305.
[21] Brindley GW. In: Brindley GW, Brown G, editors. Order-disorder in clay mineral structures. London: Mineralgical Society; 1980. p. 125–97.
[22] Ijdo WL, Pinnavaia TJ. J Solid State Chem 1998;139:281–9.
[23] Arndt UW. J Appl Cryst 1986;19:145–63.
[24] Osman MA, Mittal V, Lusti HR. Macromol Rapid Commun 2004;25(12):1145–9.
[25] Bharadwaj RK. Macromolecules 2001;34(26):9189–92.
[26] Vermogen A, Masenelli-Varlot K, Séguéla R, Duchet-Rumeau J, Bouchard S, Prele P. Macromolecules 2005;38:9661–9.
[27] Solomon DH, Hawthorne DG. Chemistry of pigments and fillers. New York: Wiley; 1983. p. 8.
[28] Yano K, Usuki A, Okada A. J Polym Sci Part A Polym Chem 1997;35:2289.
[29] Lan T, Kaviratna PD, Pinnavaia TJ. Chem Mater 1994;6:573.
[30] Giannelis EP. Adv Mater 1996;8:29.
[31] Xu RJ, Manias E, Snyder AJ, Runt J. Macromolecules 2001;34:337.
[32] Nielsen LE. J Macromol Sci. (Chem) 1967;A1:929.
[33] Cussler EL, Hughes SE, Ward III WJ, Aris R. J Membr Sci 1988;38:161.
[34] Fredrickson GJ, Bicerano J. J Chem Phys 1999;110:2181.
[35] Gusev AA, Lusti HR. Adv Mater 2001;13:1641.
[36] Lusti HR, Gusev AA, Guseva O. Model Simul Mater Sci Eng 2004;12:1201–7.
[37] Osman MA, Mittal V, Morbidelli M, Suter UW. Macromolecules 2004;37:7250.
[38] Osman MA, Mittal V, Lusti HR. Macromol Rapid Commun 2004;25:1145.
[39] Nawani P, Gelfer MY, Hsiao BS, Frenkel A, Gilman JW, Khalid S. Langmuir 2007;23:9808–15.
[40] Ruland W, Tompa H. Acta Cryst A 1968;24:93.
[41] Ruland W. Collid Polym Sci 1977;255:833.
[42] Onsager L. Ann N Y Acad Sci 1949;51:627.
[43] Hermans JJ, Hermans PH, Vermaas D, Weidinger A. Recl Trav Chim Pays-Bas-J Roy Neth Chem Soc 1946;65:427.
[44] Hanley HJM, Muzny CD, Butler BD. Langmuir 1997;13:5276–82.